



# Zero-field superconducting diode effect in small-twist-angle trilayer graphene

Jiang-Xiazi Lin<sup>1,7</sup>, Phum Siriviboon<sup>1,7</sup>, Harley D. Scammell<sup>2</sup>, Song Liu<sup>3</sup>, Daniel Rhodes<sup>3</sup>, K. Watanabe <sup>0,4</sup>, T. Taniguchi <sup>0,5</sup>, James Hone <sup>0,3</sup>, Mathias S. Scheurer <sup>0,6</sup> and J.I.A. Li <sup>0,1</sup> <sup>∞</sup>

The critical current of a superconductor can be different for opposite directions of current flow when both time-reversal and inversion symmetry are broken. Such non-reciprocal behaviour creates a superconducting diode and has recently been experimentally demonstrated by breaking these symmetries with an applied magnetic field or by the construction of a magnetic tunnel junction. Here we report an intrinsic superconducting diode effect that is present at zero external magnetic field in mirror-symmetric twisted trilayer graphene. Such non-reciprocal behaviour, with sign that can be reversed through training with an out-of-plane magnetic field, provides direct evidence of the microscopic coexistence between superconductivity and time-reversal symmetry breaking. In addition to the magnetic-field trainability, we show that the zero-field diode effect can be controlled by varying the carrier density or twist angle. A natural interpretation for the origin of the intrinsic diode effect is an imbalance in the valley occupation of the underlying Fermi surface, which probably leads to finite-momentum Cooper pairing and nematicity in the superconducting phase.

s was noticed very early on in the field of superconductivity $^{1-3}$ , time-reversal symmetry  $\Theta$  is a key ingredient in the formation of a superconductor. This follows from the fact that within the Bardeen-Cooper-Schrieffer theory and for most known superconductors, Cooper pairs form between Kramers partners, whose degeneracy is the fundamental reason why so many systems become superconductors at sufficiently low temperatures. By the same token, breaking  $\Theta$ —by applying a magnetic field, as a consequence of magnetic impurities, or spontaneously at a magnetic instability—suppresses the superconducting state. Since the advent of unconventional superconductivity, the possibility that more exotic superconducting order parameters, beyond the Bardeen-Cooper-Schrieffer paradigm, can survive and coexist with magnetic order has attracted substantial attention to this day. For example, sufficiently strong magnetic fields can give rise to the Fulde-Ferrell-Larkin-Ovchinnikov (FFLO) state<sup>4,5</sup> where the centre-of-mass momentum of Cooper pairs is non-zero, leading to a spatially modulated order parameter. Although the existence of non-uniform, FFLO-like states has been well established by bringing a superconductor and a ferromagnet in close vicinity<sup>6</sup> and the evidence of FFLO states in applied magnetic fields have been reported<sup>7,8</sup>, the microscopic coexistence between superconductivity and ferromagnetism remains rare<sup>9-15</sup>.

Recently, an experimental study<sup>16</sup> demonstrated the non-trivial interplay of superconducting current and magnetic field, which attracted substantial attention<sup>17-19</sup>. It is shown that the magnetic-field-induced broken time-reversal symmetry together with the lack of an inversion centre in the system give rise to non-reciprocal supercurrents. This exotic phenomenon, often referred to as the superconducting diode effect, is manifested in an asymmetric current–voltage curve, where the superconducting critical current is different along opposite directions of d.c. current

flow. Up to now, non-reciprocal transport behaviour that is intrinsic to the superconductor has only been demonstrated in the presence of an external magnetic field<sup>16,20–22</sup>. The realization of robust superconducting non-reciprocity at zero magnetic field would provide direct evidence for the microscopic coexistence between superconductivity and spontaneous time-reversal symmetry breaking.

In this work, we report the experimental observation of the zero-field superconducting diode effect in twisted trilayer graphene (tTLG). Figure 1a highlights two distinct twist-angle regimes, which are marked with different colours. Out of the five samples studied in this work (Supplementary Table 3 provides a list of samples), the zero-field superconducting diode effect is only observed in the small-twist-angle regime around  $\theta$ =1.3°, which is well below the expected magic angle. We note that an atomic interface between tTLG and a thin crystal of tungsten diselenide (WSe<sub>2</sub>) does not change the main phenomenology of our observation. We focus our discussion here on the behaviour and tunability of the zero-field diode effect in sample A, which has a twist angle of  $\theta$ =1.25°, and leave the influence of the tTLG/WSe<sub>2</sub> interface to a separate discussion elsewhere

In sample A, a robust superconducting phase emerges in the density range of  $2 < \nu_{\rm tTLG} < 4$  (Fig. 1b). It occupies a portion of the phase space in the  $\nu_{\rm tTLG} - D$  map (Fig. 1c, dark blue). The temperature dependence of longitudinal resistance  $R_{\rm xx}$  shows a sharp superconducting transition at around T=1 K (Fig. 1d). Notably, critical temperature  $T_{\rm c}$  is not substantially suppressed compared with previous measurements near the magic angle, despite the fact that  $\theta=1.25^{\circ}$  is well below the magic angle. Figure 1e plots the current–voltage (I-V) characteristics measured at zero magnetic field (B=0) after field training in a positive magnetic field.

We see that the critical current of the superconducting phase, defined as the d.c. current bias at the onset of longitudinal

<sup>1</sup>Department of Physics, Brown University, Providence, RI, USA. <sup>2</sup>School of Physics, the University of New South Wales, Sydney, New South Wales, Australia. <sup>3</sup>Department of Mechanical Engineering, Columbia University, New York, NY, USA. <sup>4</sup>Research Center for Functional Materials, National Institute for Materials Science, Tsukuba, Japan. <sup>5</sup>International Center for Materials Nanoarchitectonics, National Institute for Materials Science, Tsukuba, Japan. <sup>6</sup>Institute for Theoretical Physics, University of Innsbruck, Innsbruck, Austria. <sup>7</sup>These authors contributed equally: Jiang-Xiazi Lin, Phum Siriviboon. <sup>™</sup>e-mail: jia\_li@brown.edu

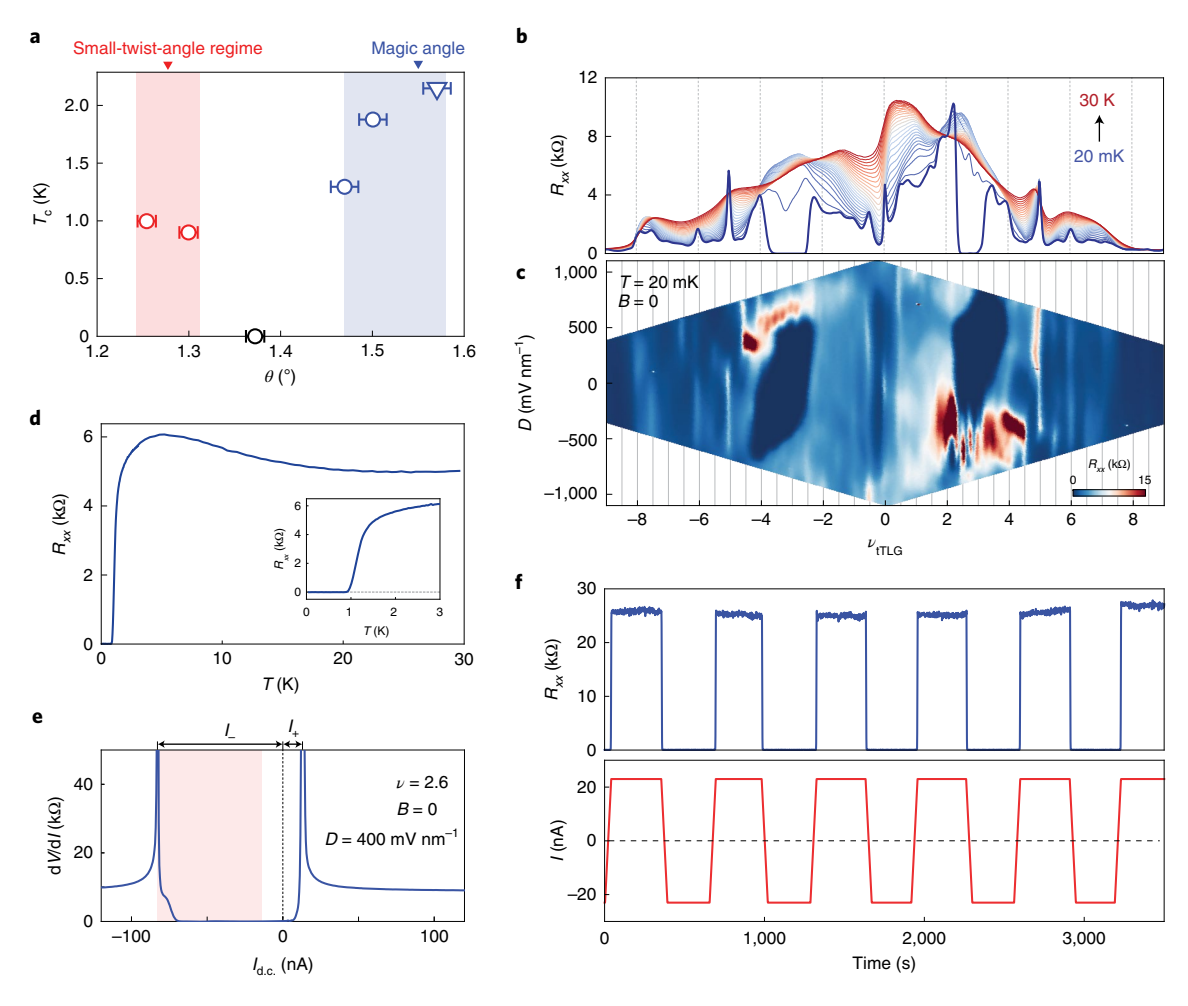
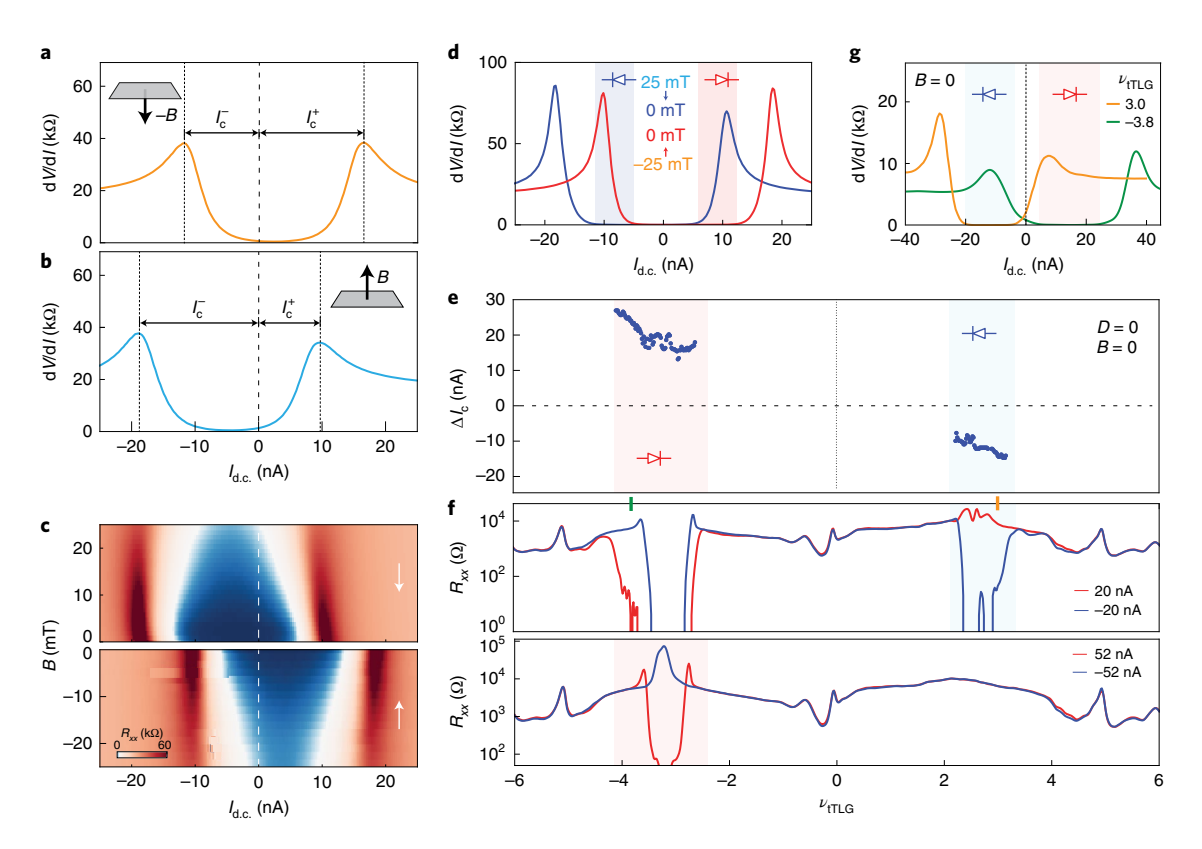


**Fig. 1** | Superconductivity and zero-field superconducting diode effect. **a**, Twist-angle dependence of the superconducting transition temperature. The horizontal error bars represent the twist angle uncertainty of each sample. The twist-angle range near the magic angle is marked with the blue-shaded area, whereas the small-twist-angle regime is shown in red. The triangle is taken from elsewhere<sup>31</sup>. **b**, Longitudinal resistance  $R_{xx}$  as a function of moiré filling measured at D=0, B=0 and different temperatures. **c**, Longitudinal resistance  $R_{xx}$  as a function of D and moiré filling  $v_{tTLG}$  measured at B=0 and T=20 mK. **d**, T=20 mK. **d**,

resistance, is highly direction dependent. The non-reciprocal component of the critical current  $\Delta I_c = I_c^+ - I_c^-$ , where  $I_c^+$  and  $I_c^-$  are the critical currents with a positive and negative d.c. bias, respectively, is non-zero—the defining feature of the zero-field superconducting diode effect. Since the critical current is much larger under a negative d.c. current bias, the superconducting phase acts like a reverse diode in the d.c. current range of  $-I_c^- < I_{\rm d.c.} < -I_c^+$  (Fig. 1e, shaded area). Notably, the zero-field superconducting diode effect is non-volatile. As the d.c. current bias varies between +22 and -22 nA, the sample alternatively switches between the superconducting and normal-state behaviour over a time span of more than an hour (Fig. 1f).

The presence of either time-reversal ( $\Theta$ ) or two-fold rotation ( $C_{2z}$ ) symmetry implies that  $\Delta I_c = 0$  (Supplementary Section 1). As such, our observation of non-reciprocal behaviour provides unambiguous evidence that both  $C_{2z}$  and  $\Theta$  are broken in the superconducting state. To provide additional evidence for the spontaneous breaking of  $\Theta$  and its coexistence with superconductivity, we next demonstrate that the diode effect can be reversed through training

with an external magnetic field. Figure 2a,b shows that the sign of  $\Delta I_c$  correlates with the B-field direction in the presence of an out-of-plane magnetic field. As the magnetic field is slowly reduced to zero, the superconducting phase maintains the same non-reciprocity (Fig. 2c), giving rise to a hysteretic behaviour where the sign of  $\Delta I_c$  is determined by the field-training history (Fig. 2d). After field training with positive (negative) B, the superconducting phase behaves like a reverse (forward) diode in the current range of  $-I_c^- < I_{d.c.} < -I_c^+$  ( $I_c^- < I_{d.c.} < I_c^+$ ). The fact that the zero-field non-reciprocity can be reversed through field training reveals that the underlying time-reversal-symmetry-breaking order can efficiently couple to an out-of-plane magnetic field, which provides important constraints on the order parameter<sup>23</sup> (Supplementary Section 1): for instance, an in-plane spin polarization cannot be efficiently trained with an out-of-plane field; therefore, the underlying time-reversal symmetry breaking more probably arises from valley polarization or out-of-plane spin-polarization. Irrespective of the microscopic origin of the diode effect, it is an emergent property of a moiré system, since none of the component materials are magnetic.



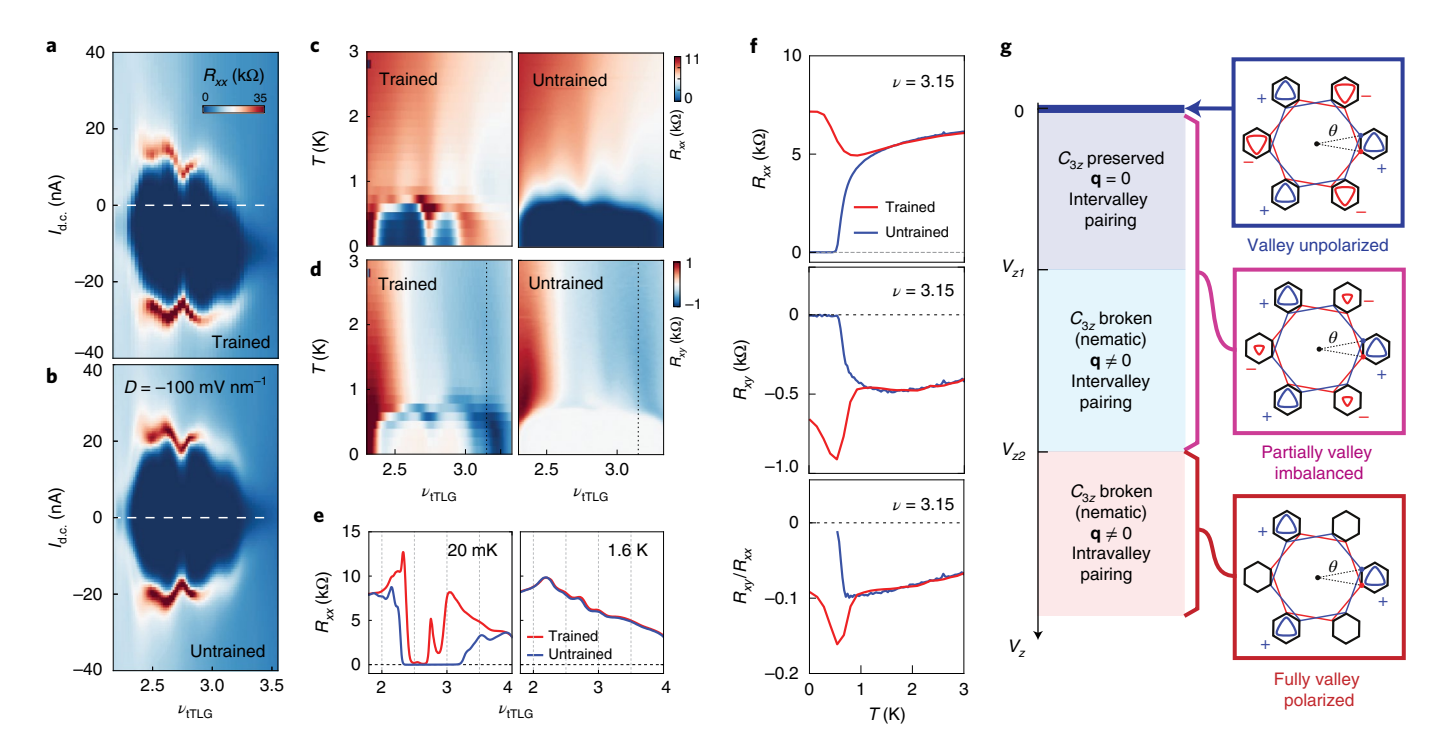
**Fig. 2 | Controlling the superconducting diode effect. a,b**, Differential resistance dV/dl as a function of d.c. current  $I_{dc}$  at  $D=-573\,\mathrm{mV}\,\mathrm{nm}^{-1}$ ,  $\nu_{\mathrm{tTLG}}=2.14$  and  $T=20\,\mathrm{mK}$ . The measurement is performed at  $B=-25\,\mathrm{mT}$  (a) and  $B=25\,\mathrm{mT}$  (b). c,  $dV/dl-I_{dc}-B$  map. The vertical white arrow marks the direction in which the magnetic field is swept. d, Differential resistance dV/dl as a function of d.c. current  $I_{dc}$  measured at B=0,  $T=20\,\mathrm{mK}$ ,  $D=-573\,\mathrm{mV}\,\mathrm{nm}^{-1}$  and  $\nu_{\mathrm{tTLG}}=2.14$ . The blue and red traces are measured after field training at  $B=+25\,\mathrm{and}\,-25\,\mathrm{mT}$ , respectively. e, Non-reciprocal component of critical current  $\Delta I_c$  versus  $\nu_{\mathrm{tTLG}}$  measured at B=0 and D=0. This measurement is performed following a sequence of steps: train the diode effect with a positive magnetic field (i); set the external magnetic field to zero (ii); measure the I-V characteristics at different carrier densities (iii). Non-reciprocity is extracted from these I-V curves. f,  $R_{xx}$  as a function of moiré filling measured at D=0, B=0 and  $T=20\,\mathrm{mK}$ , after field training with a positive magnetic field. The measurement is performed with an a.c. modulation of 1nA on top of a d.c. current bias of  $\pm 20\,\mathrm{nA}$  (top) and  $\pm 52\,\mathrm{nA}$  (bottom). g, Differential resistance dV/dI as a function of d.c. current  $I_{dc}$  measured at D=0,  $T=20\,\mathrm{mK}$  and different  $\nu_{\mathrm{tTLG}}$  values, as indicated.

Figure 2e reveals an extra experimental knob to control the non-reciprocity of superconducting transport behaviour without having to train the sample using an external magnetic field. After field training with a positive external magnetic field, we show that the sign of the zero-field superconducting diode effect can be reliably and repeatedly switched by changing the charge carrier polarity via field-effect doping. This observation suggests that the spontaneous time-reversal-symmetry-breaking field underlying the diode effect remains robust as the sample is tuned outside the superconducting density range. This provides strong indication that time-reversal symmetry breaking arises from the underlying Fermi surface of the normal phase<sup>23</sup> (Extended Data Fig. 1). In addition, Fig. 2f shows that the superconducting diode effect persists in the entire density range of the superconducting phase. After field training with a positive external magnetic field, the entire density range of the electron-doped (hole-doped) superconducting phase behaves like a reverse (forward) diode, and the sample exhibits dissipationless behaviour at  $I_{d.c.} = -20 \,\text{nA}$  ( $I_{d.c.} = +52 \,\text{nA}$ ) but appears highly resistive at  $I_{d.c.} = +20 \,\text{nA}$  ( $I_{d.c.} = -52 \,\text{nA}$ ). The uniform response across the entire density range is consistent with a diode effect intrinsic to the superconducting phase, which is distinct from the non-reciprocity arising from a magnetic tunnel junction<sup>24</sup> or Josephson networks<sup>25</sup>. As such, we have realized a junction-free superconductor film, which operates as a supercurrent diode and achieves the one-way transport of electrical charge without power

consumption. Notably, the density dependence of  $\Delta I_{\rm c}$  (Fig. 2e) gives rise to extreme non-reciprocity near the high-density end of the superconducting regime. In this regime, the sample is resistive at  $I_{\rm d.c.}=0$ , but exhibits dissipationless transport behaviour when  $I_{\rm d.c.}$  is non-zero (Fig. 2g). Such extreme non-reciprocity provides further confirmation for a robust diode effect that is intrinsic to the superconducting phase.

Although the superconducting diode effect can be stabilized by training with a non-zero magnetic field, it can also be suppressed using a large d.c. current on the order of  $200\,\mathrm{nA}$  (Fig. 3a,b). The influence of the d.c. current probably originates from the dynamics of domain formation under a large current bias (Extended Data Fig. 2 and Supplementary Information). Our ability to 'train' and 'untrain' the non-reciprocity offers a unique opportunity to examine transport behaviours that are directly associated with the superconducting diode effect. For instance, the 'trained' configuration exhibits an apparent increase in both longitudinal and Hall resistance around the transition temperature  $T_c$ , which is defined as the temperature where  $R_{xx}$  in the untrained configuration diminishes. As superconductivity is destroyed at higher temperature ( $T > T_c$ ), the influence of training and untraining diminishes (Fig. 3e).

This shows that the underlying time-reversal-symmetry-breaking order is only a rather weak perturbation to the band structure and, for example, does not induce insulating behaviour or completely polarize a flavour degree of three of the system (such as the valley or



**Fig. 3 | Possible origin of the zero-field superconducting diode effect. a, b**, Differential resistance as a function of moiré filling  $v_{\text{tTLG}}$  and d.c. bias current measured at  $T = 20 \,\text{mK}$  and  $B = 0 \,\text{mT}$ . The measurement is performed with the superconducting diode effect after field training (**a**) and without the diode effect after 'untraining' with a large d.c. current (**b**). **c, d**,  $R_{xx}$  (**c**) and  $R_{xy}$  (**d**) as a function of temperature T and  $v_{\text{tTLG}}$  measured with (left) and without (right) the superconducting diode effect. The measurement is performed with a small a.c. current bias of  $I = 1 \,\text{nA}$  at  $B = 0 \,\text{and} \, D = 0 \,\text{mV} \,\text{nm}^{-1}$ . **e**,  $R_{xx}$  as a function of  $v_{\text{tTLG}}$  with (red trace) and without (blue trace) the superconducting diode effect. The measurement is performed with a small a.c. current bias of  $I = 1 \,\text{nA}$  at  $B = 0 \,\text{nd} \, T = 20 \,\text{mK}$  (left) and  $T = 1.6 \,\text{K}$  (right). The superconducting diode effect induces dramatic changes in  $R_{xx}$  at  $T < T_c$ , but has no influence at  $T > T_c$ . **f**, Temperature dependence of  $R_{xx}$  (top),  $R_{xy}$  (middle) and  $R_{xy}/R_{xx}$  (bottom) taken at  $v_{\text{tTLG}} = 3.15$ , which is marked by the dashed lines in **c** and **d**. **g**, Schematic of the moiré Brillouin zone and Fermi surfaces. Valley polarization induces an imbalance between the Fermi surfaces in valley  $+ 1 \,\text{m} \, \text{m} \, \text$ 

spin quantum number) at a temperature substantially larger than  $T_c$ ; this is consistent with the fact that superconductivity can coexist with it, as required for the zero-field diode effect. At the same time, the increase in  $R_{xy}$  leads to an enhanced ratio of  $R_{xy}/R_{xx}$  compared with the normal state at higher temperatures (Fig. 3f). The enhancement in the ratio of  $R_{xy}/R_{xx}$  indicates that time-reversal ( $\Theta$ ) or three-fold rotational ( $C_{3z}$ ) symmetry is broken (Supplementary Section 4). Since the enhanced  $R_{xy}/R_{xx}$  disappears as the non-reciprocity is suppressed in the 'untrained' configuration, the reduced symmetry is probably directly associated with the superconducting diode effect.

Notably, the superconducting behaviour at a small current bias is observed over a larger (smaller) density range in the absence (presence) of the non-reciprocal behaviour (Fig. 3c,d). It is worth pointing out that the variation in the superconducting density range results from the extreme non-reciprocity in the high-density regime, where dissipationless transport is only robust with non-zero d.c. bias current (Figs. 2g and 3a–d). On the other hand, Extended Data Fig. 2b shows that  $(I_+ + I_-)/2$  remains the same despite the onset of the zero-field diode effect, providing a strong indication that the robustness of the superconducting phase is not influenced by the process of field training.

Given the abundance of orbital ferromagnetism in graphene moiré systems, a natural explanation for the zero-field diode effect and its associated symmetry breaking is an interaction-induced imbalance in the valley occupation of the underlying Fermi surface. The spontaneous formation of an imbalance of electrons in the two

valleys breaks both  $C_{2z}$  and  $\Theta$ , providing the necessary symmetry requirement for the emergence of a zero-field superconducting diode effect. As such, a valley-imbalanced Fermi surface, in theory, can give rise to non-reciprocal superconducting transport behaviour in the absence of proximity-induced spin-orbit coupling (SOC). However, the presence of (at least Ising) SOC is required for the valley order to couple to an external out-of-plane magnetic field (Supplementary Table 2)<sup>23</sup>. In sample A, the SOC could result from the proximity effect with the WSe<sub>2</sub> crystal, which explains the observed field trainability discussed above (Supplementary Section 5 and Extended Data Fig. 3 provide more details regarding the influence of the proximity effect).

An imbalance in the valley occupation of the underlying Fermi surface has crucial consequences for the superconducting state<sup>23</sup>. Let us denote the degree of valley imbalance by  $V_z$ , which can be qualitatively thought of as the difference in chemical potentials in the two valleys. At  $V_z$ =0, a valley-balanced Fermi surface preserves time-reversal symmetry (Fig. 3g, top blue square). In this scenario, the two valleys are related by reversing the sign of the crystalline momentum  $\mathbf{k} \rightarrow -\mathbf{k}$ , making intervalley pairing at zero centre-of-mass momentum ( $\mathbf{q}$ =0) the most favourable. In the presence of non-zero valley polarization ( $V_z \neq 0$ ), this Kramers degeneracy is lifted. In general, a valley-imbalanced Fermi surface reduces the superconducting transition temperature. But if a superconducting phase survives, it is expected to exhibit the zero-field diode effect. Notably, there are two critical values in the valley polarization  $V_z$ .

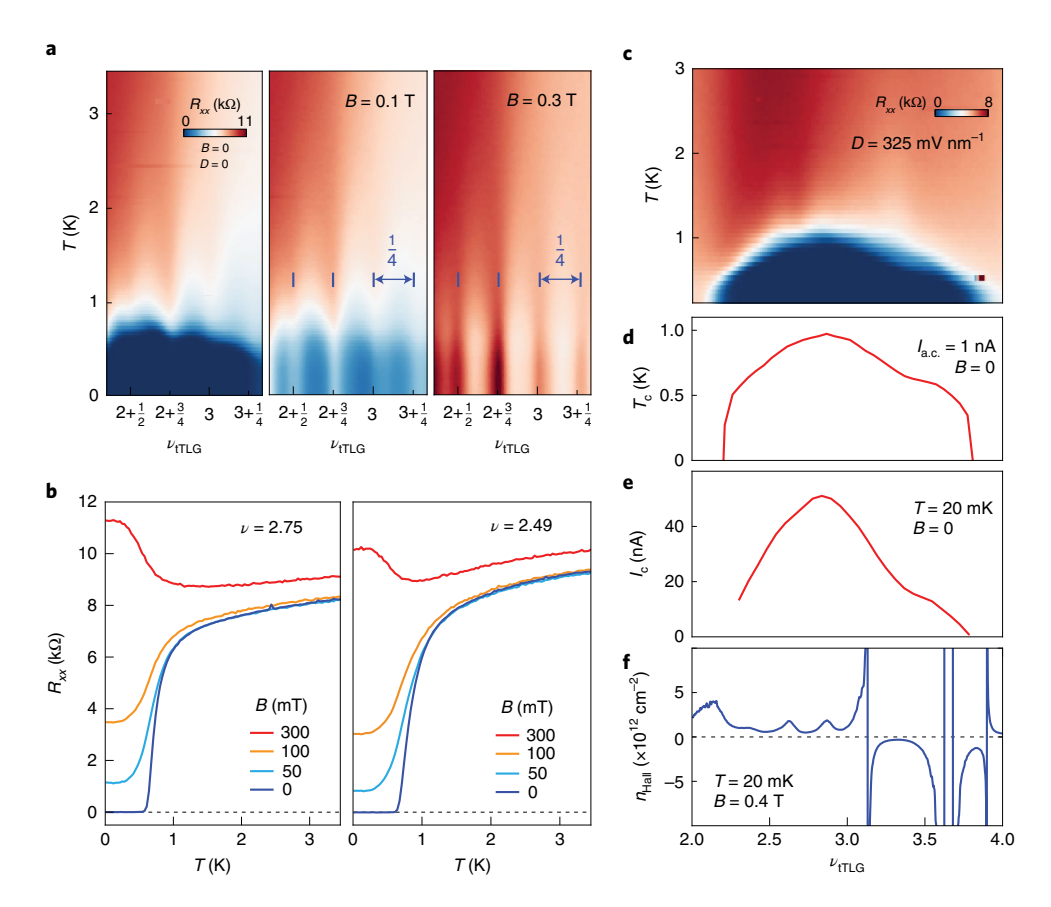


**Fig. 4 | DWs and superconductivity. a**,  $v_{1TLG} - T$  map of  $R_{xx}$  measured at different B values. The vertical blue bars in the right panels mark 1/4 period in moiré filling. **b**,  $R_{xx}$  as a function of T measured at v = 2.75 (left) and v = 2.49 (right) for different B values. The data in **c-f** are measured for the electron pocket at  $D = 325 \, \text{mV nm}^{-1}$ . **c**,  $R_{xx}$  as a function of temperature and filling. **d**, Critical temperature extracted from **b**. **e**, Critical current at 20 mK and 0 T. **f**, Hall density ( $n_{\text{Hall}}$ ) at 20 mK and 0.4 T.

For a finite range of  $V_z$  around zero, the associated Cooper pairs exhibit a vanishing centre-of-mass momentum q=0 as a consequence of  $C_{3z}$ . This results in a critical value of valley imbalance  $V_{z1}$ , below which the  $C_{3z}$  symmetry is preserved (Fig. 3g, blue region) and Cooper pairs form with zero centre-of-mass momentum (q = 0). At  $V > V_{z1}$ , valley imbalance gives rise to Cooper pairing and non-zero centre-of-mass momentum appears ( $\mathbf{q} \neq 0$ ). This finite-momentum pairing state also breaks  $C_{3z}$ . Given the extreme non-reciprocity (Fig. 2g), sample A probably falls inside this regime of valley imbalance, at least for certain  $\nu_{\text{tTLG}}$ . It is worth pointing out that the resulting nematicity also provides a natural explanation for the enhancement in  $R_{ry}/R_{rx}$  in the trained configuration (Supplementary Section 4). Given the partial valley imbalance, the observed variation in  $\Delta I_c$ offers a direct characterization for the density dependence of  $V_z$  in the underlying Fermi surface. According to Fig. 2e,g,  $V_z$  is maximized at a large carrier density.

Further increasing the valley imbalance results in a fully valley-polarized Fermi surface at  $V_z = V_{z2}$  (Fig. 3g, red square). A sufficiently large valley imbalance also requires Cooper pairs to form within the same valley. Such intravalley pairing gives rise to extremely large centre-of-mass momentum, of the scale of the Brillouin zone of individual graphene layers, rendering the superconducting phase highly unstable. This offers a natural explanation for the absence of the zero-field diode effect near the magic angle (Extended Data Fig. 4). Owing to the dominating influence of flavour polarization near the magic angle, the Fermi surface near  $\nu = \pm 2$  is either perfectly valley balanced ( $V_z = 0$ ) or fully valley polarized ( $V_z = V_{z2}$ ) (Fig. 3g, red region). As a result, the observed

superconducting phase near the magic angle is always associated with an underlying Fermi surface, which preserves time-reversal symmetry, and  $\Delta I_c$ =0 by symmetry. Combined, the absence of the zero-field diode effect near the magic angle suggests that the suppressed influence of flavour polarization and partial imbalance in valley occupation are key to stabilize the non-reciprocal supercurrents in the small-twist-angle regime<sup>26</sup>.

Notwithstanding the good agreement between the valleypolarization-based mechanism for the diode effect and the observed phenomenology, we note that from a purely symmetry perspective, it is also possible that the normal state of the superconductor is non-magnetic but  $\Theta$  is spontaneously broken at the superconducting transition<sup>23,27</sup>. Indeed, there is exactly one candidate pairing state23 that our system can reach by a single continuous phase transition that has the correct symmetries. Transforming under a non-trivial representation of the point group (E of  $C_{3z}$ ), this state is expected to be fragile against impurities in the system and hence represents a less natural option than valley polarization. As it breaks  $\Theta$ , it can only be stabilized by fluctuations of a time-reversal odd collective mode, such as spin fluctuations, and not by phonons alone<sup>28</sup>; as such, future Coulomb screening experiments<sup>29,30</sup> should be able to clarify the mechanism underlying the diode effect. Given that non-reciprocal superconducting transport is observed at B = 0, it is unlikely to be associated with exotic vortex dynamics. The microscopic coexistence between superconductivity and time-reversal symmetry breaking offers the most natural explanation for the mechanism underlying this exotic transport behaviour. Nevertheless, a definitive identification of such coexistence

will require the direct characterization of time-reversal symmetry breaking, which is beyond the scope of this work.

In the following, we will investigate the relationship between superconductivity and density-wave (DW) instabilities. Moiré energy bands are populated by DW phases in the small-twist-angle regime<sup>26</sup> in a range of  $\nu_{\rm tTLG}$  and D that overlaps with that of superconductivity (Fig. 1c). This is demonstrated in Fig. 4a by the density modulation of 1/4 moiré filling in  $R_{xx}$  as superconductivity is suppressed by external magnetic field B. Interestingly, the melting temperature of DW approximately coincides with  $T_c$  of the superconducting phase (Fig. 4b), suggesting that the underlying energy scale is comparable between superconductivity and DW order. As such, it is important to address the connection between these two phenomena. In particular, we have to distinguish between two different scenarios: (1) DW order and superconductivity coexist microscopically, that is, on decreasing B, Cooper pairs form in the minibands reconstructed by the DW order; (2) superconductivity and DW order are competing ground states and DW order disappears at the onset of superconductivity (and vice versa). To this end, we will compare the density dependence of superconductivity at B=0 and of the DW states at B=0.4 T. At D=325 mV nm<sup>-1</sup>, the Hall density measured at  $B = 0.4 \,\mathrm{T}$  exhibits a complex density modulation of 1/4 moiré filling, with several divergences in the range of  $3 < \nu_{\text{tTLG}} < 4$  (Fig. 4f), which are associated with DW-induced band reconstruction<sup>26</sup>. Regardless of its pairing symmetry, the strength of superconductivity, reflected by quantities such as  $T_c$  and  $I_c$ , is generically expected to be sensitive to changes in the density of states of the parent Fermi surface. However, the critical temperature  $T_c$  and critical current  $I_c$  of the superconducting phase at B=0 vary smoothly with  $\nu_{\rm tTLG}$  (Fig. 4d,e). The fact that the superconducting phase is largely unaffected by DW-induced changes in the density of states indicates that DW states at 0.4 T are not the parent state of superconductivity. This favours scenario (2) over (1) and superconductivity and DW are more probably competing orders. In this case, the magnetic order responsible for the diode effect, such as the valley polarization discussed above, is an additional instability, distinct from the DW order. We note that superconductivity and DW phases may coexist at the base temperature of  $T \approx 20 \,\mathrm{mK}$  in certain parts of the phase space, which gives rise to extreme anisotropic transport behaviour in the superconducting phase (Supplementary Fig. 3).

Last, we comment on the twist-angle dependence of the superconducting phase in tTLG (refs. <sup>26,30-32</sup>). As shown in a recent experimental work<sup>26</sup>, the interplay between Coulomb correlation and superconductivity in the small-twist-angle regime takes a form distinct from the magic angle. In the small-twist-angle regime (Fig. 1a, red-shaded area), a lack of hierarchy between the correlation-driven phases indicates that the influence of flavour polarization is substantially diminished26. This provides a key ingredient for realizing the zero-field diode effect: a partial imbalance in the valley occupation of the underlying Fermi surface. Consistently, we found zero-field non-reciprocity in the superconducting state in two small-twist-angle samples (Extended Data Fig. 5 shows the data from sample B). On the other hand, partial valley polarization is found to be unfavourable near the magic angle, owing to the dominating influence of flavour polarization. Combined, this provides a natural explanation for twist-angle dependence of the zero-field diode effect discussed here. Taken together, this establishes the small-twist-angle regime in tTLG as a novel paradigm for correlated physics, which involves the complex interplay of superconductivity, broken time-reversal symmetry, finite-momentum pairing and DW instabilities.

# Online content

Any methods, additional references, Nature Research reporting summaries, source data, extended data, supplementary information, acknowledgements, peer review information; details of

author contributions and competing interests; and statements of data and code availability are available at https://doi.org/10.1038/s41567-022-01700-1.

Received: 14 May 2022; Accepted: 29 June 2022; Published online: 15 August 2022

#### References

- Ginzburg, V. Ferromagnetic superconductors. Sov. Phys. JETP-USSR 4, 153–160 (1957).
- Matthias, B., Suhl, H. & Corenzwit, E. Spin exchange in superconductors. Phys. Rev. Lett. 1, 92–94 (1958).
- 3. Anderson, P. Theory of dirty superconductors. *J. Phys. Chem. Solids* 11, 26–30 (1959)
- Fulde, P. & Ferrell, R. A. Superconductivity in a strong spin-exchange field. Phys. Rev. 135, A550–A563 (1964).
- Larkin, A. & Ovchinnikov, Y. N. Nonuniform state of superconductors. Sov. Phys.-JETP 20, 762 (1965).
- Buzdin, A. I. Proximity effects in superconductor-ferromagnet heterostructures. Rev. Mod. Phys. 77, 935–976 (2005).
- Bianchi, A., Movshovich, R., Capan, C., Pagliuso, P. G. & Sarrao, J. L. Possible Fulde-Ferrell-Larkin-Ovchinnikov superconducting state in CeCoIn<sub>5</sub>. Phys. Rev. Lett. 91, 187004 (2003).
- Radovan, H. A. et al. Magnetic enhancement of superconductivity from electron spin domains. *Nature* 425, 51–55 (2003).
- Felner, I., Asaf, U., Levi, Y. & Millo, O. Coexistence of magnetism and superconductivity in R<sub>1.4</sub>Ce<sub>0.6</sub>RuSr<sub>2</sub>Cu<sub>2</sub>O<sub>10-δ</sub>(R = Eu and Gd). *Phys. Rev. B* 55, R3374–R3377 (1997).
- Aoki, D. et al. Coexistence of superconductivity and ferromagnetism in URhGe. Nature 413, 613–616 (2001).
- 11. Pfleiderer, C. et al. Coexistence of superconductivity and ferromagnetism in the *d*-band metal ZrZn<sub>2</sub>. *Nature* **412**, 58–61 (2001).
- Ren, Z. et al. Superconductivity induced by phosphorus doping and its coexistence with ferromagnetism in EuFe<sub>2</sub>(As<sub>0.7</sub>P<sub>0.3</sub>)<sub>2</sub>. Phys. Rev. Lett. 102, 137002 (2009).
- Dikin, D. A. et al. Coexistence of superconductivity and ferromagnetism in two dimensions. *Phys. Rev. Lett.* 107, 056802 (2011).
- Li, L., Richter, C., Mannhart, J. & Ashoori, R. Coexistence of magnetic order and two-dimensional superconductivity at LaAlO<sub>3</sub>/SrTiO<sub>3</sub> interfaces. Nat. Phys. 7, 762–766 (2011).
- Bert, J. A. et al. Direct imaging of the coexistence of ferromagnetism and superconductivity at the LaAlO<sub>3</sub>/SrTiO<sub>3</sub> interface. *Nat. Phys.* 7, 767–771 (2011).
- Ando, F. et al. Observation of superconducting diode effect. Nature 584, 373–376 (2020).
- 17. Yuan, N. F. & Fu, L. Supercurrent diode effect and finite-momentum superconductors. *Proc. Natl Acad. Sci. USA* 119, e2119548119 (2022).
- Daido, A., Ikeda, Y. & Yanase, Y. Intrinsic superconducting diode effect. *Phys. Rev. Lett.* 128, 037001 (2022).
- He, J. J., Tanaka, Y. & Nagaosa, N. A phenomenological theory of superconductor diodes. New J. Phys. 24, 053014 (2022).
- Ichikawa, F. et al. Asymmetric critical currents of Nb and YBCO thin films for the polarity of the transport current in parallel magnetic fields. *Physica C Supercond.* 235, 3095–3096 (1994).
- Jiang, X., Connolly, P., Hagen, S. & Lobb, C. Asymmetric currentvoltage characteristics in type-II superconductors. *Phys. Rev. B* 49, 9244–9247 (1994).
- Broussard, P. & Geballe, T. Critical currents in sputtered Nb-Ta multilayers. Phys. Rev. B 37, 68–74 (1988).
- Scammell, H. D., Li, J. & Scheurer, M. S. Theory of zero-field superconducting diode effect in twisted trilayer graphene. 2D Mater. 9, 025027 (2022).
- Diez-Merida, J. et al. Magnetic Josephson junctions and superconducting diodes in magic angle twisted bilayer graphene. Preprint at https://arxiv.org/ abs/2110.01067 (2021).
- Hooper, J. et al. Anomalous Josephson network in the Ru-Sr<sub>2</sub>RuO<sub>4</sub> eutectic system. *Phys. Rev. B* 70, 014510 (2004).
- Siriviboon, P. et al. Abundance of density wave phases in twisted trilayer graphene on WSe<sub>2</sub>. Preprint at https://arxiv.org/abs/2112.07127v1 (2021).
- Zinkl, B., Hamamoto, K. & Sigrist, M. Symmetry conditions for the superconducting diode effect in chiral superconductors. Preprint at https:// arxiv.org/abs/2111.05340 (2021).
- Scheurer, M. S. Mechanism, time-reversal symmetry, and topology of superconductivity in noncentrosymmetric systems. *Phys. Rev. B* 93, 174509 (2016).
- Liu, X. et al. Tuning electron correlation in magic-angle twisted bilayer graphene using Coulomb screening. Science 371, 1261–1265 (2021).

- 30. Liu, X., Zhang, N. J., Watanabe, K., Taniguchi, T. & Li, J. Isospin order in superconducting magic-angle twisted trilayer graphene. *Nat. Phys.* **18**, 522–527 (2022).
- 31. Park, J. M., Cao, Y., Watanabe, K., Taniguchi, T. & Jarillo-Herrero, P. Tunable strongly coupled superconductivity in magic-angle twisted trilayer graphene. *Nature* **590**, 249–255 (2021).
- 32. Hao, Z. et al. Electric field–tunable superconductivity in alternating-twist magic-angle trilayer graphene. *Science* **371**, 1133–1138 (2021).
- 33. Serlin, M. et al. Intrinsic quantized anomalous Hall effect in a moiré heterostructure. *Science* **367**, 900–903 (2020).
- 34. Lin, J.-X. et al. Spin-orbit-driven ferromagnetism at half moiré filling in magic-angle twisted bilayer graphene. *Science* 375, 437–441 (2022).

**Publisher's note** Springer Nature remains neutral with regard to jurisdictional claims in published maps and institutional affiliations.

© The Author(s), under exclusive licence to Springer Nature Limited 2022

# Data availability

Source data are provided with this paper.

### Acknowledgements

J.-X.L. and J.I.A.L. acknowledge funding from NSF DMR-2143384. Device fabrication was performed in the Institute for Molecular and Nanoscale Innovation at Brown University. P.S. acknowledges support from the Brown University Undergraduate Teaching and Research Awards. M.S.S. acknowledges funding from the European Union (ERC-2021-STG, Project 101040651 - SuperCorr). Views and opinions expressed are however those of the authors only and do not necessarily reflect those of the European Union or the European Research Council. Neither the European Union nor the granting authority can be held responsible for them. H.D.S. acknowledges funding from the ARC Centre of Excellence FLEET. K.W. and T.T. acknowledge support from the Elemental Strategy Initiative conducted by the MEXT, Japan (grant number JPMXP0112101001), and JSPS KAKENHI (grant numbers 19H05790, 20H00354 and 21H05233).

#### **Author contributions**

J.-X.L. and P.S. fabricated the devices and performed the measurements. J.-X.L., P.S. and J.I.A.L. analysed the data. J.-X.L., P.S., H.D.S., M.S.S. and J.I.A.L. wrote

the article. K.W. and T.T. provided the hBN crystals. S.L., D.R. and J.H. provided the WSe, crystals.

## **Competing interests**

A provisional patent application has been filed by Brown University under Serial No. 63/289,563. The inventors include J.I.A.L., J.L., P.S. and M.S.S. The application, which is pending, contains proposals of two-dimensional material architecture designed for realizing the zero-field superconducting diode effect.

#### Additional information

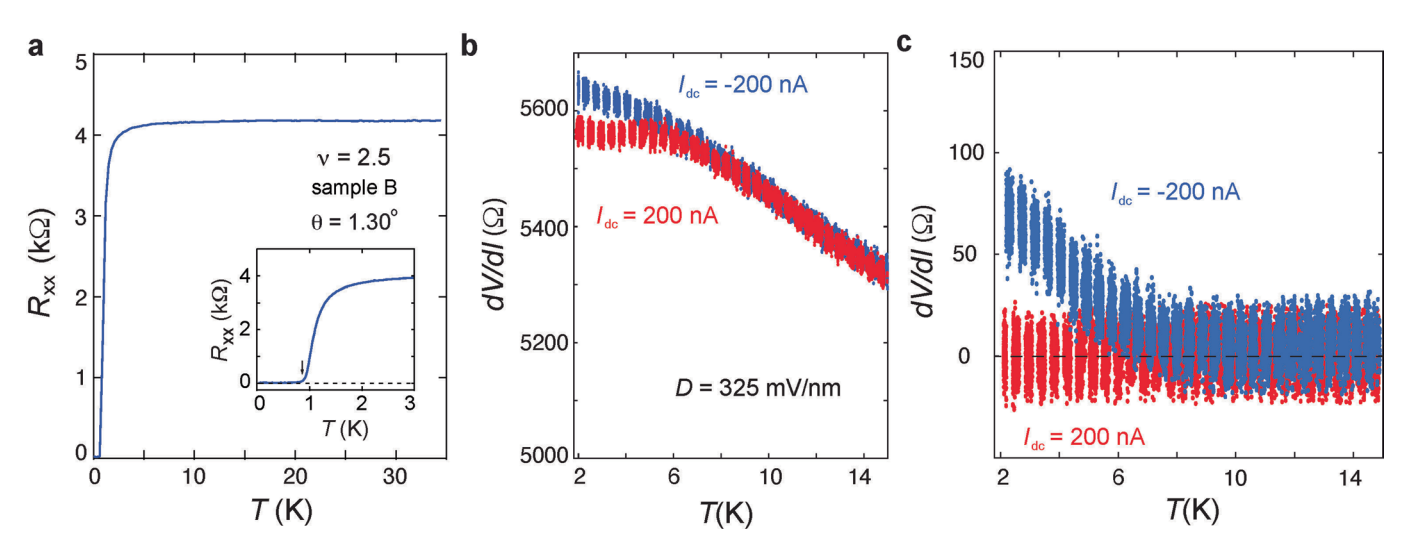
Extended data is available for this paper at https://doi.org/10.1038/s41567-022-01700-1.

**Supplementary information** The online version contains supplementary material available at https://doi.org/10.1038/s41567-022-01700-1.

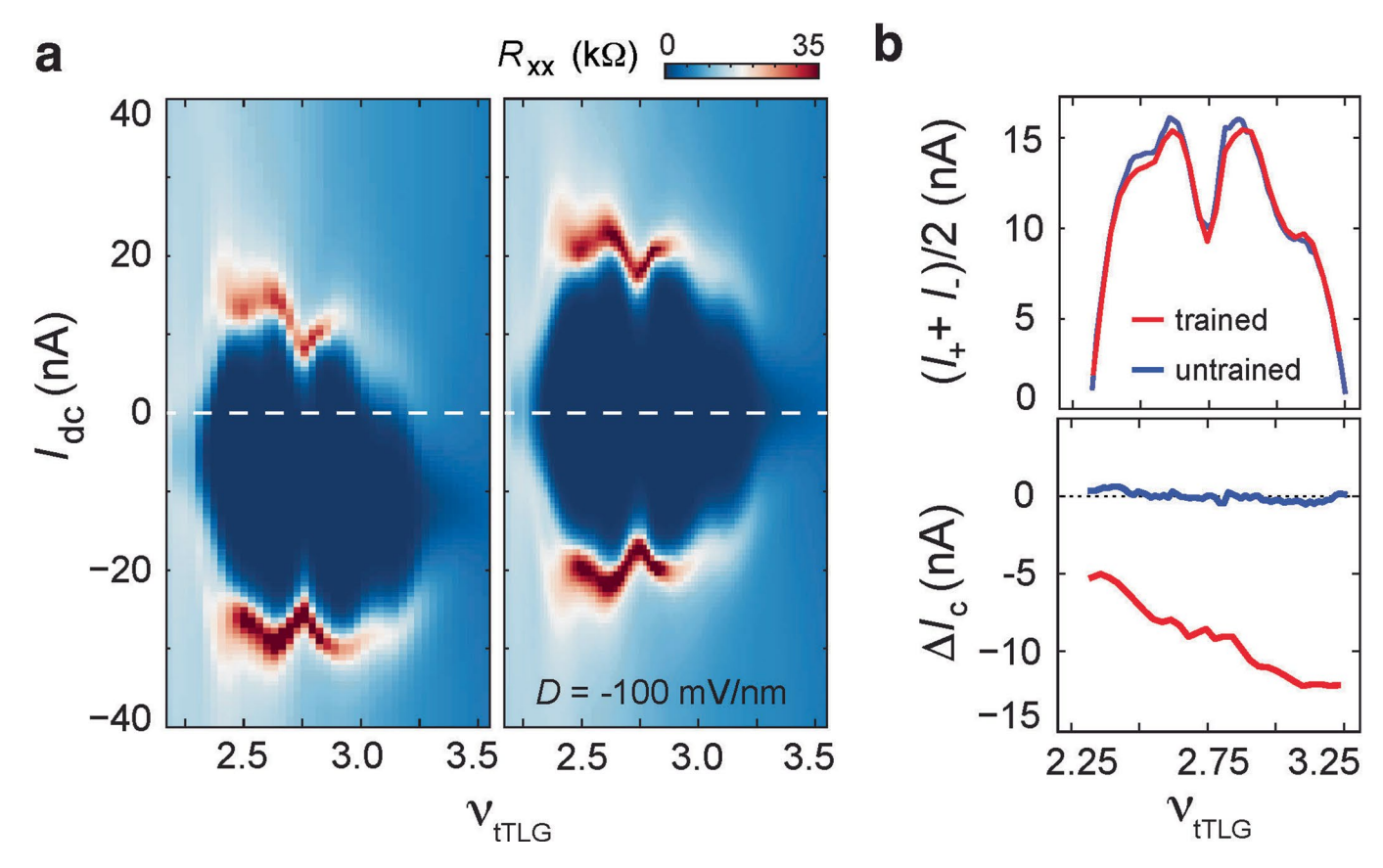
Correspondence and requests for materials should be addressed to J.I.A. Li.

Peer review information  $Nature\ Physics$  thanks the anonymous reviewers for their contribution to the peer review of this work

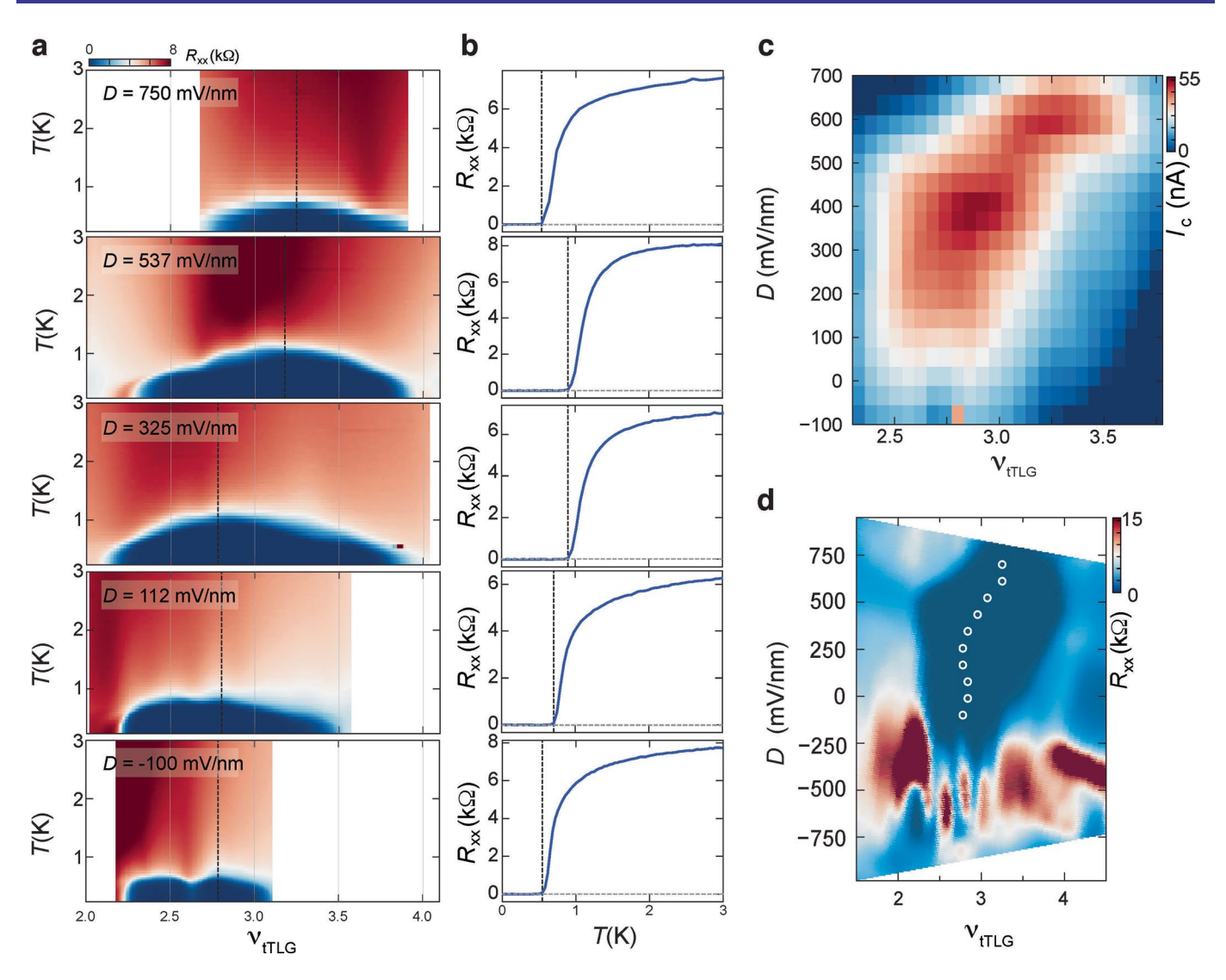
Reprints and permissions information is available at www.nature.com/reprints.



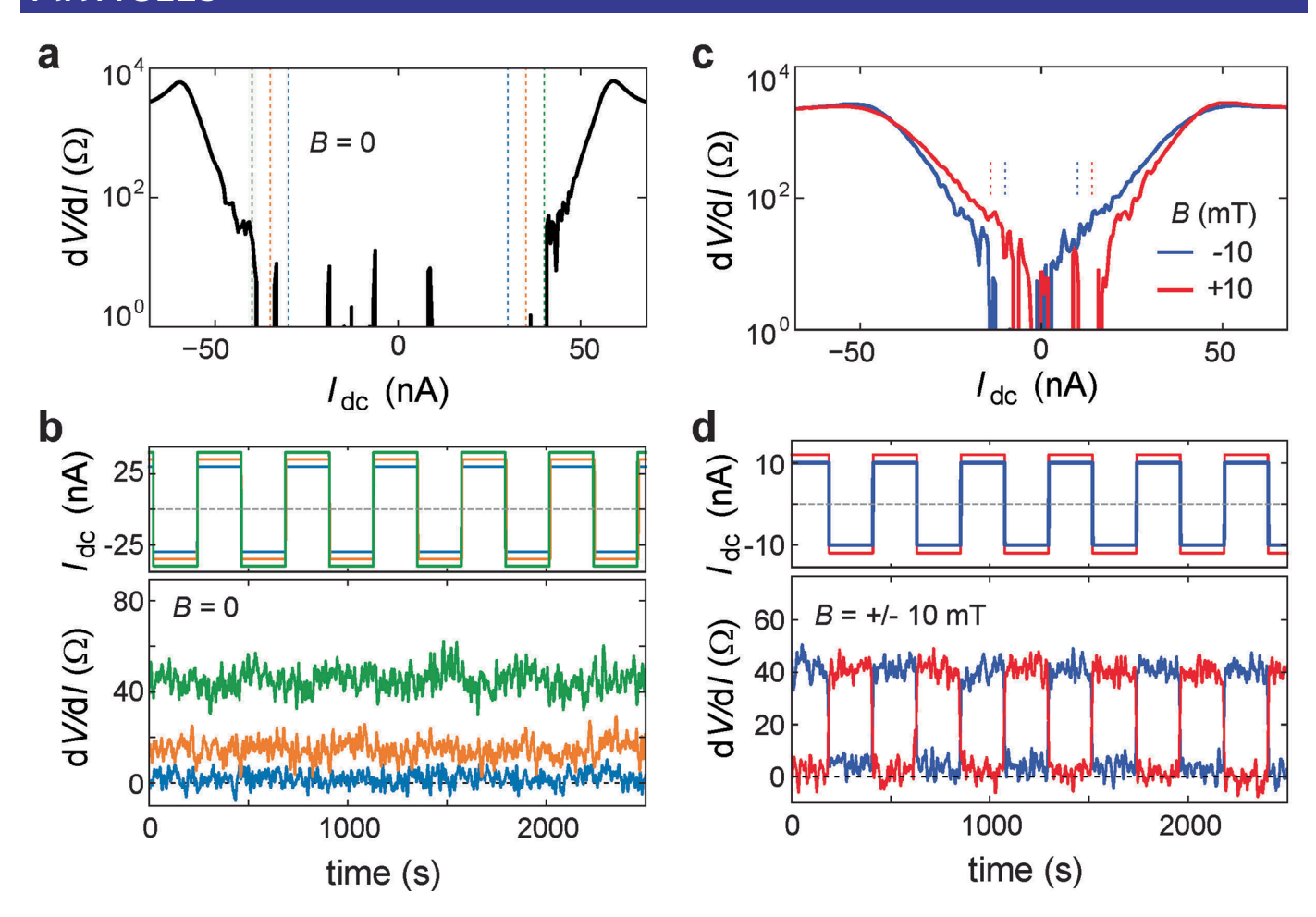
Extended Data Fig. 1 | Weak nonreciprocity in normal state transport in sample B. a,  $R_{xx}$  versus T measured at B=0 and  $\nu_{tTLG}=2.5$  in sample B.  $T_c$  is around 0.95 K, defined by the onset in  $R_{xx}$  with increasing temperature. b, dV/dI measured with  $I_{dc}=\pm 200$  nA (red dots) and -200 nA (blue dots) as a function of temperature in the temperature range  $T>T_c$ . c, Renormalized dV/dI showing the difference between  $I_{dc}=\pm 200$  nA as a function of T. The difference in dV/dI between  $I_{dc}=\pm 200$  nA is around  $50\Omega$ , which is consistent with the very weak nonreciprocity at  $I_{dc}>I_c$  at low temperature (Extended Data Fig. 5b). This nonreciprocity decreases with increasing temperature and completely vanishes at T>6 K. This observation is consistent with an underlying fermi surface with partial valley imbalance, which simultaneously breaks time-reversal and inversion symmetries. The valley imbalance, hence time-reversal symmetry breaking, onsets spontaneously at  $T\approx 6$  K. Even though time-reversal and inversion symmetries are broken in the normal state, nonreciprocity is greatly enhanced by the onset of the superconducting phase.



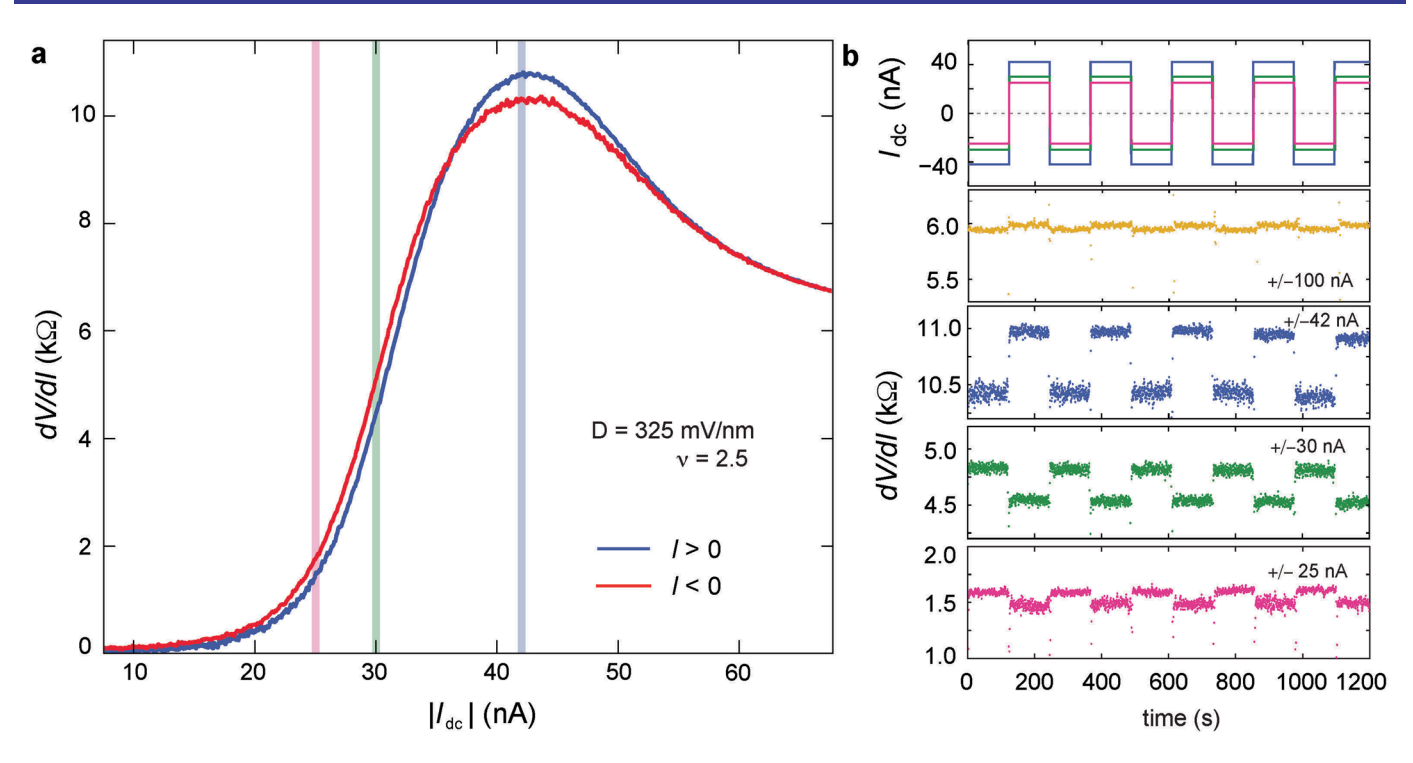
**Extended Data Fig. 2** | The robustness of superconductivity in trained and untrained configurations. **a**, dV/dI as a function of  $I_{dc}$  and  $\nu_{tTLG}$  measured at B=0 and D=-100 mV/nm for the electron doped superconducting phase. The measurement is performed with the superconducting diode effect after field training (left panel), and without the superconducting diode effect after 'un-training' with a large DC current (right panel). **b**, The reciprocal (top panel) and non-reciprocal (bottom panel) component of the critical current,  $(I_c^+ + I_c^-)/2$  and  $\Delta I_{cr}$  as a function of  $\nu_{tTLG}$  extracted from **a**. It is worth noting that several experimental works have reported interplay between DC current flow and the sign of magnetic order: in orbital ferromagnetic states, a large DC current is shown to induce sign-reversal in the magnetic order  $^{33,34}$ . It is hypothesized that the mechanism underlying current-induced switching stems from the interaction between different magnetic domains and current flow around the edge of the domain. Our observation that a large DC current couples to the underlying time-reversal symmetry is consistent with previous experimental results. However, the sample interior of an orbital ferromagnet is insulating and current flows along the edge of the magnetic domain. Whereas the sample interior in the nonreciprocal superconducting phase is highly conductive. As such, we anticipate the interplay between DC current and the underlying time-reversal symmetry breaking to be different. Notably, how DC current interacts with the magnetic order remains an open question for graphene moiré systems in general  $^{33,34}$ .



**Extended Data Fig. 3** | Optimal doping and critical temperature dependence on displacement field. **a,b**, Longitudinal resistance  $R_{xx}$  as a function of filling fraction  $\nu_{tTLG}$  and temperature. The optimal doping is indicated via dash lines in **a**, and the temperature dependence at optimal doping is plotted in **b**. **c,d**, Critical current  $I_c$  as a function of filling fraction  $\nu_{tTLG}$  and displacement field D. The optimal doping for each displacement field is plotted in **d** overlaying with the  $R_{xx}$  map. Both the temperature and the dc current dependence suggest the increase in optimal doping as the displacement field increases.



**Extended Data Fig. 4 | The absence of zero-field superconducting diode effect near the magic angle. a**, Differential resistance dV/dI as a function of  $I_{dc}$  measured at B=0, T=20 mK and  $\nu_{tTLG}=-2.64$  for Sample C. The I-V curve is symmetric with DC bias current. **b**, Current switching experiment taken at the same condition as in **a**. DC current bias is switched between positive and negative 30 nA (blue), 35 nA (orange) and 40 nA (green). No difference in resistance is observed for different current directions, in either superconducting or normal states. **c**, dV/dI as a function of  $I_{dc}$  measured at B=-10 mT (blue trace) and +10 mT (red trace). **d**, Current switching experiment taken at the same condition as in **c**. DC current bias is switched between + -10 nA at B=-10 mT (blue), and + -14 nA at B=+10 mT (red). The non-reciprocity in the presence of a symmetry breaking field shows a superconducting diode effect. The fact that superconducting diode effect is absent at B=0 shows that time reversal symmetry is preserved in both the normal and superconducting phase in sample C. This is distinctly different compared to the observation in sample A.



Extended Data Fig. 5 | Zero-field superconducting diode effect in sample B. a, Differential resistance dV/dl as a function of DC current bias l<sub>dc</sub> measured at B=0, T=20 mK and  $\nu_{tTIG}=2.5$ . The blue vertical stripe marks the peak position in the differential resistance,  $I_{ct}$  where the superconducting phase transitions into normal state behaviour. Blue and red traces denote measurement with positive and negative DC current bias, respectively. The fact that dV/dl measured with different signs of DC current deviate from each other points towards zero-field nonreciprocity in the superconducting transport behaviour. Notably, the nonreciprocity diminishes as DC current exceeds the critical current I<sub>c</sub>. **b**, dV/dI measured with alternating DC current bias at  $\pm$  100nA,  $\pm$  42nA,  $\pm$  30 nA and  $\pm$  25 nA. Nonreciprocity is apparent in the DC current range of  $I_{dr} < I_{cr}$ . Above the critical current  $I_{cr}$  nonreciprocity is substantially suppressed. This observation suggests that the fermi surface underlying the superconducting phase is partially valley imbalanced. In this scenario, time-reversal and inversion symmetries are simultaneously broken in the normal state, and SOC is not required to enable zero-field superconducting diode effect. However, the presence of SOC could still enhance the nonreciprocity through the following mechanisms: (i) SOC enhances the valley polarization in the partially valley imbalanced fermi surface 34, which gives rise to a more pronounced nonreciprocity in the zero-field superconducting transport behaviour; (ii) according to a recent theoretical work<sup>23</sup>, the presence of the SOC is essential for the trainability of the zero-field superconducting diode effect. Without the SOC-induced trainability, the sample is expected to have multiple domains of opposite valley polarization, diminishing the observed nonreciprocity. These expectations are consistent with our measurement result, where the zero-field diode effect is much weaker in the sample without WSe<sub>2</sub>. Since two samples do not offer statistical significance to confirm the influence of SOC on the robustness of the zero-field diode effect, we will leave a more systematic discussion on the influence of WSe, to a separate work. It is worth noting that the collection of samples studied in our work is sufficient to confirm the main phenomenology, which is the interplay between orbital ferromagnetism, superconductivity, and Coulomb correlation.